A MEMS viscometer for unadulterated human blood

Article (Accepted Version)

A MEMS viscometer for unadulterated human blood

Abbreviated Title: MEMS viscometer for human blood

P.D. Smith, R.C.D. Young, C.R. Chatwin*,

School of Science and Technology, University of Sussex, Falmer, Brighton, BN1 9QT.

*Corresponding author: Tel =+44(0)1273 678901 E-mail address: c.r.chatwin@sussex.ac.uk

Abstract

The design and theoretical modelling of an oscillating micro-mechanical-viscometer designed for the measurement of whole unadulterated human blood, is described. The proposed device utilises the dependence of the squeeze-film damping ratio on properties of the surrounding fluid to measure fluid viscosity using an oscillating plate structure. The optimum geometrical configuration for the device structure has been investigated and a methodology for defining the optimum configuration of the micro-mechanical sensor identified. This is then applied to calculate the predicted noise equivalent viscosity change $\mathrm{NE}\Delta\eta$. It was found that the device performance is limited by electronic noise within the detection circuitry rather than thermal mechanical noise. An electronic noise limited measurement resolution of $\leq 0.11\%$, is predicted for measurement over a shear range of $1.0 \rightarrow 1000\mathrm{s}^{-1}$, at a measurement bandwidth of $50\mathrm{Hz}$. The linearity of response of the micro-mechanical-viscometer is considered and the device is predicted to provide a linear measurement response.

Keywords: MEMS, Viscosity, Squeeze-Film Damping, Rheology, Human Blood.

1 Introduction

There is increasing clinical interest in the measurement of the viscosity of whole unadulterated human blood as an aid to the diagnosis of cardiovascular conditions.[1],[2] In particular, it has been shown that measurements of the viscosity of whole unadulterated human blood may be useful in mapping hyperlipidemic and hypertensive states.[3] Because of the inherently long measurement times associated with conventional viscometers, it is generally necessary to add anti-coagulants to human blood to prevent clotting. Conventional viscometers also have the added disadvantage that they require relatively large sample volumes. To successfully measure the viscosity of whole unadulterated human blood a faster viscometer is required, with a smaller sample volume and wider shear range than that offered by conventional technology.

Alternative capillary-tube viscometers have been proposed that are capable of measuring whole blood viscosity without the need for anticoagulants. These include, the scanning capillary-tube viscometer, Rheolog^{TM}, and a mass-detecting capillary-tube viscometer.[4],[5],[6],[7],[8] Whilst recognising the effectiveness of the aforementioned capillary-tube viscometers in overcoming the main limitations of conventional viscometer technology, it is believed that MEMS (micro-elctro-mechanical systems) technology should be capable of providing a faster viscometer with a higher measurement resolution and a wider, more selective shear range.

Many different types of micro-mechanical mechanical viscometers, utilising a wide range of different measurements techniques, have been reported. These include, measurement of the torsional vibration of an oscillating tube, acoustic wave sensors,

thickness shear mode resonators, and oscillating fibre sensors.[9],[10],[11],[12],[13]

Some of the earliest work using an oscillating microstructure for measuring viscosity was carried out by Andrews et.al.[14] This work clearly demonstrated that, the phase angle between the driving force and resulting motion of an oscillating microstructure may be related to the viscosity of the gas via an expression for the squeeze-film damping ratio of the microstructure. Using a similar methodology, the principle of measuring the viscosity of a viscous fluid was later demonstrated by Oden et.al.[15] These results suggest the possibility of measuring viscosities of liquids and gases, in the range $10^{-2}\,\mathrm{Pa}\cdot\mathrm{s}$ to $10^{2}\,\mathrm{Pa}\cdot\mathrm{s}$, using a single cantilever structure.

Following on from these initial studies, several successful attempts have been made at measuring the viscosity of Newtonian and Non-Newtonian fluids with oscillating microstructures, using a variety of actuation and measurement techniques.[16],[17],[18],[19] In general these viscometers rely on separate actuation and measurement techniques, with shear being applied independently to the measurement of fluid viscosity.

It is envisaged that a fully integrated viscometer, capable of measuring viscosity whilst simultaneously applying a known yet variable shear rate, would be advantageous. The proposed micro-mechanical viscometer attempts to achieve this being a single integrated device, designed around a fluid cell that incorporates an oscillating element. It is envisaged that a driving voltage may be applied to the oscillating element to provide electrostatic actuation. The resulting motion of the oscillating element may then be measured using capacitive sensing techniques. The motion of the oscillating

element will apply shear to the fluid, whilst simultaneously providing a means of quantifying the fluid viscosity. Fluid viscosity may then be quantified, as a function of the squeeze-film damping ratio, from a direct measurement of the phase angle between the applied driving frequency and the resulting steady state motion of the oscillating bi-material plate.

2 Theory

The proposed micro-mechanical viscometer is based upon the oscillating microstructure shown in figure 1.

Figure (1) Schematic diagram of the bi-material plate structure used for the micro-mechanical viscometer, showing (a) the top view of sensor looking down on the upper gold coating layer and (b) the cross section of the side of the sensor showing all constituent layers.

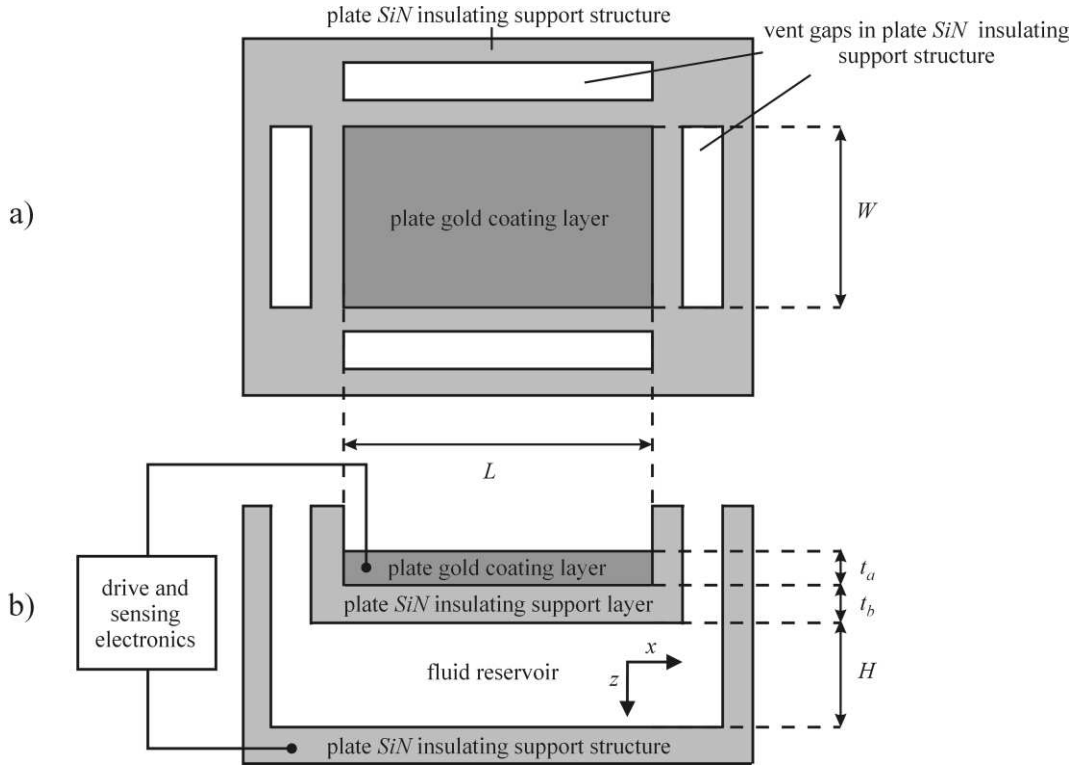

This structure forms two parallel rectangular plates with the measured fluid being held between these plates. The lower plate is held stationary, while the upper plate undergoes forced damped harmonic oscillation through the application of an electrostatic driving force. The upper bi-material plate is comprised of an insulating support layer, formed from SiN (silicon nitride), with an upper Au (gold) coating layer. L is the length and W the width of the plate. The suffixes a and b are used to denote the gold coating layer and the SiN support layer respectively. Moreover, υ_a and υ_b are the Poisson's ratio and ρ_a and ρ_b the density of the corresponding layer material. The fluid undergoing measurement is contained in a reservoir between the two plates and is completely insulated from any electrical contacts by the SiN layers. The vent holes serve a dual purpose, firstly they allow the loading of a sample fluid into the reservoir; secondly they allow free movement of the fluid in all directions.

The natural resonance frequency of the oscillating bi-material plate has been calculated by approximating its behaviour using the model of a thin rectangular plate, that is simply supported along its four edges. The natural resonance frequency of the fundamental mode of vibration is then given by,[20]

$$\omega_0 = \pi^2 \left(\frac{1}{L^2} + \frac{1}{W^2} \right) \sqrt{\frac{R}{\rho_a t_a + \rho_b t_b}} \qquad (1.)$$

where R is the flexural rigidity which is described by,

$$R = \frac{EI_{eq}}{\left(1-\upsilon_{eq}^2\right)} \tag{2.}$$

EI_{eq} is the equivalent modulus of rigidity per unit area of the bi-material plate and this has been derived using an equivalent width technique.[21] υ_{eq} is the equivalent Poisson's ratio, for the bi-material plate and this is given by,[22]

$$\upsilon_{eq} = \upsilon_a \frac{k_{3P}}{k_{2P}} \tag{3.}$$

Where k_{2P} and k_{3P} are fitting constants, which are defined as,

$$k_{2P} = 1 + \frac{E_b t_b^3\left(1-\upsilon_a^2\right)}{E_a t_a^3\left(1-\upsilon_b^2\right)} + \frac{3\left(1-\upsilon_a^2\right)\left(1+t_b/t_a\right)^2\left(1+E_a t_a/E_b t_b\right)}{\left(1+E_a t_a/E_b t_b\right)^2 - \left(\upsilon_a + \upsilon_b E_a t_a/E_b t_b\right)^2} \tag{4.}$$

$$k_{3P} = 1 + \frac{\upsilon_b E_b t_b^3\left(1-\upsilon_a^2\right)}{\upsilon_a E_a t_a^3\left(1-\upsilon_b^2\right)} + \frac{3\left(1-\upsilon_a^2\right)\left(1+t_b/t_a\right)^2\left(1+\upsilon_b E_a t_a/\upsilon_a E_b t_b\right)}{\left(1+E_a t_a/E_b t_b\right)^2 - \left(\upsilon_a + \upsilon_b E_a t_a/E_b t_b\right)^2} \tag{5.}$$

At any point on the surface of the plate the vertical displacement is assumed to be of the form,[23]

$$z(x, y) = z_0 \sin\frac{n\pi x}{L} \sin\frac{n\pi x}{W} \tag{6.}$$

where n is an integer value and x is defined as the horizontal position along the plate, measured from the boundary between the plate and the support structure.

For the fundamental mode of vibration, equation (6) predicts that the maximum vertical displacement will occur at the centre of the plate. The spring constant has been

evaluated at this point as,

$$k_s = LW\left(\rho_a t_a + \rho_b t_b\right)\omega_0^2 \qquad (7.)$$

It is assumed that the bi-material plate is subjected to a harmonic driving force of the form $F(t) = F_0 \sin \omega_E t$, where F_0 is the amplitude of the applied driving force, and ω_E the applied driving frequency.

This driving force will result in the plate exhibiting forced damped harmonic motion. Upon a change in this driving force the time varying vertical displacement of this harmonic motion, $z(t)$, contains both transient and steady state components. The transient component is expected to decay exponentially with time, and is considered negligible for $Dt/2m_{eff} > 5$, where D is the damping constant.[24] From this, the time required to reach steady state has been defined in terms of a transient decay time constant,

$$\tau_{tr} = 5/\xi\omega_0 \qquad (8.)$$

Where ξ is the damping ratio for the system,.

Upon reaching steady state conditions a forced damped harmonic oscillation, with amplitude z_0, oscillating at frequency ω_E, will exist. The time varying displacement of the bi-material plate is then defined by,

$$z(t) = z_0\left(\sin \omega_E t - \phi\right) \qquad (9.)$$

where ϕ is the phase angle between the applied driving frequency and the resulting steady state motion of the oscillating bi-material plate. This phase angle is given by,

$$\tan\phi = \frac{2\xi\,\omega_{\mathrm{E}}/\omega_0}{1-\omega_{\mathrm{E}}^2/\omega_0^2} \tag{10.}$$

The region between the bi-material plate and the fixed bottom plate is referred to as the squeeze gap and the distance between the plates is referred to as the gap height, H. When the gap height is sufficiently small, squeeze-film damping is expected to be the dominant damping mechanism. All edges in the proposed structure are considered to be vented, therefore Blech's formulation for parallel rectangular plates, is assumed to provide a valid solution for the squeeze-film damping effect.[25] For a real viscous fluid, the viscosity is expected to be independent of the ambient air pressure.[26] The expression for the squeeze-film damping ratio may then be expressed as,

$$\xi_{\mathrm{squeeze}} \approx \frac{0.402\eta_{\mathrm{eff}}\,\mathrm{L}^3\mathrm{W}}{\mathrm{m}\omega_0\mathrm{H}^3}\,\frac{\left(1+\mathrm{L}^2/\mathrm{W}^2\right)}{\left[\left(1+\mathrm{L}^2/\mathrm{W}^2\right)^2+0.010\sigma^2\right]} \tag{11.}$$

Where σ is the squeeze number given by,

$$\sigma = \frac{12\eta_{\mathrm{eff}}\,\mathrm{L}^2}{\mathrm{P}_{\mathrm{air}}\mathrm{H}^2}\,\omega_{\mathrm{E}} \tag{12.}$$

η_{eff} the shear rate dependent effective viscosity of the fluid and $\mathrm{P}_{\mathrm{air}}$ the ambient air pressure assumed to be $101.32\mathrm{kPa}$. Assuming σ is small, the ambient air pressure is expected to have virtually negligible impact on the squeeze-film damping ratio.

Thermal-mechanical noise is expected to be the main source of random noise displacements for the bi-material plate. The rms (root mean squared) random noise displacement of the bi-material plate due to thermal-mechanical noise may be described by,[27],[28],[29]

$$\left\langle z_{thermal} \right\rangle = \sqrt{\frac{4m\omega_0 k_B T_{amb} \Delta f}{m^2 Q\left[\left(\omega_0^2 - \omega_E{}^2\right)^2 + \left(\omega_0 \omega_E / Q\right)^2\right]}} \tag{13.}$$

Where Δf is the measurement bandwidth in Hz and k_B is Boltzmann constant, assumed to be $1.38\times10^{-23} J\cdot K^{-1}$, T_{amb} is the ambient temperature and Q the quality factor of the oscillator which is related to the damping ratio by, $\xi = 1/2Q$.

The solution of equation (13) will depend on the applied driving frequency as such $\left\langle z_{thermal} \right\rangle$ will be minimised for the specific cases where $\omega_E << \omega_0$ or $\omega_E >> \omega_0$

$$\left\langle z_{thermal} \right\rangle = \sqrt{\frac{4k_B T_{amb} \Delta f}{k_S \omega_0 Q}} = \sqrt{\frac{8k_B T_{amb} \xi \Delta f}{k_S \omega_0}} \tag{14.}$$

The dielectric layer between the substrate and the bi-material plate consists of two separate materials, the insulating support layer, and the fluid in the squeeze gap. For a steady state forced damped harmonic oscillation, an average time varying vertical displacement of the plate is predicted. $z_0(t)$ represents the displacement at the midpoint of the plate. The effective plate separation, d_{eff}, is more closely related to the average displacement of the plate evaluated across the whole surface of the plate which has been defined as $z_{eff}(t)$. The time varying capacitance of the micro-mechanical

viscometer may be described by,

$$C(t) = \frac{\varepsilon_0 \varepsilon_{fluid} LW}{d_{eff}(t)} = \frac{\varepsilon_0 \varepsilon_{fluid} LW}{\left(H + t_b \frac{\varepsilon_{fluid}}{\varepsilon_{t_b}} - z_{eff}(t) \right)} \quad (15.)$$

ε_0 is the permittivity of free space, assumed to be $8.85\,\mathrm{pF}\cdot\mathrm{m}^{-1}$, ε_{fluid} the relative permittivity of the fluid in the squeeze gap and ε_{t_b} the relative permittivity of the SiN insulating support layer.

It is assumed that a sinusoidal drive voltage of the form $V_{in}(t) = V_0 + V_1 \sin \omega_E t$ is applied to the micro-mechanical sensor. This drive voltage causes an attractive electrostatic force, $F_{V_{in}}(t)$, between the substrate and the bi-material plate. Assuming the micro-mechanical sensor is operated in Q-drive mode,[30] and has a constant offset displacement, the average vertical deflection of the bi-material plate may be described by,

$$z_{eff}(t) = \left(1 - \frac{2}{\pi}\right)\left[z_{offset} + z_0 \sin(\omega_E t - \phi)\right] \quad (16.)$$

The constant offset displacement being given by,

$$z_{offset} = \frac{Q_0^{\,2}}{2\varepsilon_0 LWk_s} \quad (17.)$$

for a constant charge, Q_0, which is given by,

$$Q_0 = \frac{\varepsilon_0 LW}{\left(H + t_b \frac{\varepsilon_{fluid}}{\varepsilon_{t_b}} - z_{offset} \right)} \tag{18.}$$

The applied electrostatic force will cause a vertical displacement of the bi-material plate, consisting of both static and time varying components, which at the centre of the plate is described by,

$$z(t) = z_{offset} + z_0 \sin(\omega_E t - \phi) \tag{19.}$$

For one period of oscillation the applied electrostatic force will cause vertical deflection at the centre of the plate that may be described by,

$$\langle z(t) \rangle = z_{offset} + \frac{z_0 \sqrt{2}}{2} \tag{20.}$$

Moreover, this is assumed to result from an average applied driving voltage,

$$\langle V_{in} \rangle = V_0 + \frac{V_1 \sqrt{2}}{2} \tag{21.}$$

Now by applying Hooke's law the equivalent average applied electrostatic force is described by,

$$\left\langle F_{V_{in}}(t) \right\rangle = \frac{\varepsilon_0 \langle V_{in}(t) \rangle^2 A_{elec}}{2 d_{eff}^2} = k_s \langle z(t) \rangle \tag{22.}$$

The applied electrostatic force $\propto 1/d_{eff}^2$, and the spring force $\propto \langle z(t) \rangle$, therefore equation (22) will only have a stable solution for $\langle z(t) \rangle < d_{eff}/3$.[31] When $\langle z(t) \rangle > d_{eff}/3$ this

instability will cause a sudden deflection of the centre of the bi-material plate all the way down to the bottom of the squeeze gap. This sudden deflection, generally referred to in literature in terms of a threshold or pull-down voltage, is attributed to the concentration of electrostatic forces at the centre of the plate.[32]

Whole unadulterated human blood is a Non-Newtonian fluid for which the viscosity of the fluid is expected to vary with shear rate, $\dot{\gamma}$. To fully describe the shear rate dependent effective viscosity across the full range of shear rates, a Cross model has been applied. This Cross model describes the effective viscosity of a Non-Newtonian fluid as,[33]

$$\frac{\eta_{\text{eff}} - \eta_{\text{high}}}{\eta_{\text{low}} - \eta_{\text{high}}} = \frac{1}{1 + \left(\mathrm{K}^2 \dot{\gamma}^2\right)^{(1-\mathrm{n})/2}} \tag{23.}$$

where η_{low} and η_{high} are the fluid viscosities, at very low and very high shear rates, respectively and K and n are fitting constants.

The shear rate is dependent on the velocity profile of the fluid between the plates and is expected to be proportional to the applied driving frequency. In order to define an analytical expression for the shear rate, the device under consideration has been treated as a "squeeze-flow rheometer" assuming non-lubricated squeeze flow.

For a Non-Newtonian fluid squeezed between parallel circular plates of radius r, the shear rate may be closely approximated by, [34]

$$\dot{\gamma} = \left[\frac{2(2\mathrm{n}+1)}{3\mathrm{n}}\right]\left(\frac{\mathrm{u_z r}}{\mathrm{H}^2}\right) \tag{24.}$$

Where the plate velocity,

$$u_z = -dH(z)/dt = z_0 \omega_E \cos \omega_E t \,, \tag{25.}$$

By assuming that plate is sufficiently vented so as to ensure that the fluid is free to move equally in all directions equation (24) may be applied to a rectangular plate using an effective radius for a circular plate of equivalent area, $r_{eff} = \sqrt{LW/\pi}$. For a rectangular plate the rms shear rate, resulting from an rms plate velocity, $\langle u_z \rangle = z_0 \omega_E / \sqrt{2}$, may then be described by,

$$\langle \dot{\gamma} \rangle = \left[\frac{2(2n+1)}{3n} \right] \left[\left(\frac{z_0 \omega_E}{\sqrt{2} H^2} \right) \left(\frac{LW}{\pi} \right)^{1/2} \right] \tag{26.}$$

The above set of governing analytical equations has been applied in the following section to model the operation of the proposed device. Equations 1 to 10 define the analytical model applied to evaluate the motion of the oscillating plate structure. Particular attention has been paid to the relationship between the squeeze-film damping ratio and the phase angle that exists between the applied driving frequency and the resulting frequency of oscillation of a bi-material plate.

Equation 11 describes the relationship between the squeeze-film damping ratio and the viscosity of the fluid. This is applied in conjunction with the relevant results from the derivation outlined by equations 1 to 10 to define the change in phase angle that results from a change in fluid viscosity. The corresponding thermal mechanical-noise term has then been defined in equations 13 and 14.

The plate is subjected to a sinusoidal drive voltage and the resulting motion of the plate described in equations 15 to 22, of particular importance is the vertical displacement of the plate as this relates directly to shear rate applied to the fluid. Finally equations describing the effective viscosity of a Non-Newtonian fluid as a function of shear rate have been presented. In particular an equation describing the dependence of the applied shear rate on the motion of the plate and geometrical configuration of the device has been defined.

3 Device Modelling

All device modelling has been based upon an $SiN - Au$ bi-material plate structure using the assumed material parameters shown in table I.

TABLE I Assumed material parameters used for calculation of optimum viscometer configuration and resulting performance values.

Material Parameter	Gold	Silicon Nitride	Human Blood
Young's Modulus, E (GPa)	78	146	-
Density, ρ ($kg \cdot m^{-3}$)	18900	3100	-
Poisson's ratio, υ	0.35	0.28	-
Relative permittivity, ε	-	7.5	73

The bi-material plate is treated as a forced damped harmonic oscillator subject to an electrostatic driving force through application of a driving voltage applied under Q-drive conditions. The driving force is assumed to be applied at a constant frequency and the phase angle quantified from the squeeze-film damping ratio through application of equation (11).

The phase angle may only be measured once steady state conditions have been reached. The measurement bandwidth for the micro-mechanical viscometer is therefore dependent on the transient decay time constant. Since the transient decay time constant is itself dependent on the damping ratio, it is necessary to take into account the value of

$\xi_{squeeze}$ when setting the measurement bandwidth for the micro-mechanical sensor.

The performance of the proposed viscometer has been quantified in terms of $NE\Delta\eta$ (noise equivalent viscosity change). This is defined as the change in viscosity that produces an snr (signal to noise ratio) of unity. Both signal and noise will produce a change in the damping ratio through different mechanisms. Only the change in signal however, results from a change in fluid viscosity. Therefore, both signal and noise are defined in terms of a change in damping ratio, $\Delta\xi$.

The signal is derived directly from the viscosity of the fluid, with the relationship between η_{signal} and ξ_{signal} being defined by equation (11). Signal is denoted by $\Delta\xi_{signal}$, and is defined as the change in squeeze-film damping ratio that occurs due to a change in viscosity of $\Delta\eta_{signal}$.

Mechanical noise is assumed to arise solely from the change in gap height that occurs due to thermal-mechanical noise. Noise is denoted by $\Delta\xi_{noise}$ and is defined as, the change in damping ratio that occurs due to the average change in gap height that would result from $\langle z_{thermal} \rangle$, with $\langle z_{thermal} \rangle$ being calculated from equation (13). The resulting signal to noise ratio is then simply defined as, $snr = \Delta\xi_{signal} / \Delta\xi_{noise}$. Both $\Delta\xi_{signal}$ and $\Delta\xi_{noise}$ noise are calculated as deviations from the standard squeeze film damping ratio, with $\Delta\xi_{signal} = \xi_{signal} - \xi_0$ and $\Delta\xi_{noise} = \xi_{noise} - \xi_0$. Where ξ_0 is the initial squeeze-film damping ratio, associated with the effective viscosity of whole unadulterated human blood at the minimum rms shear rate, η_0.

To minimise the rms thermal-mechanical noise displacements ω_E is set at a value well above the natural resonance frequency of the bi-material cantilever. $\langle z_{thermal} \rangle$ will then be approximated by equation (14). This suggests that, $\langle z_{thermal} \rangle \propto \xi^2$ and therefore the noise, will be minimised by minimising ξ_0. This is achieved by setting the gap height at its maximum permissible value, H_{max}.

Three main restrictions that limit H_{max} have been identified. Firstly, it is necessary to ensure that squeeze-film damping remains the dominant damping source. Contributions from the fluid spring force have been neglected. It is then assumed that, as the gap height is increased, viscous damping will eventually become the dominant damping source. We therefore impose the condition that the gap height must be set small enough to ensure that $\xi_{viscous} \leq \xi_{squeeze}/10$, where the squeeze film damping ratio for viscous damping is given by,

$$\xi_{viscous} = \frac{3\pi\eta_{eff} W + \frac{3}{4}\pi W^2 \left(2\rho_{fluid}\eta_{eff}\omega_E\right)^{1/2}}{2\left(\rho_a t_a + \rho_b t_b\right) W^2 \omega_E} \qquad (27.)$$

with ρ_{fluid} being the viscosity of the surrounding fluid.

The second restriction on H_{max} arises from the need to limit the maximum permissible voltage for actuation of the bi-material cantilever. As the plates are moved further apart, the drive voltage must be increased to maintain a constant amplitude of oscillation. To account for this the condition is imposed that the gap height must be set sufficiently small so as to ensure that $V_0 \leq 100V$.

The third constraint is imposed by the dependence of the measurement bandwidth on the transient decay time constant. The transient decay time constant is dependent on the damping ratio as described by equation (8). Since the damping ratio is dependent on the gap height, the gap height must be small enough so as to ensure that the transient decay time constant is smaller than the time required for a single measurement.

Three fundamental restrictions on the minimum permissible gap height, H_{min} have also been identified. The first restriction is imposed by the pull down voltage, with the minimum gap height being identified as $H_{min} \geq 3\langle z(t)\rangle$. The second restriction on the minimum gap height arises from the need to maintain the squeeze-film damping ratio below the level of critical damping. In order to achieve this the minimum gap height must be set such that $2\xi^2 > 1$. The final restriction arises due to the existence of a cut-off squeeze number, σ_c. In order to maintain squeeze-film damping as the dominant damping mechanism the gap height must be set sufficiently large as to ensure that $\sigma \leq \sigma_c$. The cut-off squeeze number being given by,[28]

$$\sigma_C = \pi^2\left(1 + L^2/W^2\right) \tag{28.}$$

The shear rate is determined by the applied driving frequency and this driving frequency may be set at any fixed value. In order to obtain the lowest possible shear rate, and the largest range of shear rates, the driving frequency is initially set at its lowest permissible value. The minimum permissible value of ω_E is set by the measurement bandwidth. Allowing for 10 periods of oscillation within a single

measurement cycle, the chosen measurement bandwidth imposes the condition that $\omega_E \geq 20\pi\Delta f$. Since whole human blood is a shear thinning fluid, the minimum driving frequency will also correspond to the point of highest fluid viscosity. As such, the maximum measurable viscosity is evaluated at this driving frequency.

The shear rate also has a strong dependence on the gap height. In all calculations the gap height is set such the minimum rms shear rate, $\langle \dot{\gamma}_0 \rangle$, is at the chosen value when $\omega_E = 20\pi\Delta f$. Both the minimum and maximum gap heights are restricted as previously described, assuming an offset displacement of $z_{offset} = 0.1\mu m$ and an amplitude of oscillation of $z_0 = 0.1\mu m$.

4 Predicted Device Performance

The performance of the proposed micro-mechanical viscometer has been evaluated for whole unadulterated human blood, Hb 37%, assumed to have Cross-model parameters of $\eta_{low} = 0.125 Pa \cdot s$, $\eta_{high} = 0.005 Pa \cdot s$, $K = 52.5$ and $n = 0.285$.[35] In addition all calculations of the optimum sensor configuration and predicted optimum performance, assume a maximum measurement range of $\eta_0 + 20\%$ as evaluated at the minimum shear rate.

In order to determine a methodology for identifying the optimum device configuration, the impact that individual geometrical parameters have on $NE\Delta\eta$ has been investigated. It was found that the optimum configuration for the viscometer may

be identified with the driving frequency set at a value of $\omega_E = 20\pi\Delta f$ and the gap height set so as to maintain minimum shear rate at the chosen value.

Under these conditions, with t_b set at an arbitrarily chosen fixed value, simulations have shown that for any given plate length and width, $NE\Delta\eta$ will decrease as t_a increases. This decrease in $NE\Delta\eta$ with increasing t_a continues until a cut-off point is reached. Above this cut-off point the cut-off squeeze number is exceeded and no valid solution for H exists. The cut-off point therefore defines the optimum value of t_a. Because of the strong dependence of $\Delta\xi_{signal}$ and $\Delta\xi_{noise}$ on ξ_0, and hence σ, $NE\Delta\eta$ will have the same value at the cut-off point, regardless of the value of t_b. As such, t_b does not have an identifiable optimum value and may be arbitrarily set at any chosen value.

With t_a set at its optimum value, further simulations suggest that, for any fixed plate length, $NE\Delta\eta$ will decrease as the plate width is decreased. A minimum cut-off value of W is also found to exist, and this cut-off corresponds to approximately the same value irrespective of the plate length. The cut-off value therefore defines the optimum plate width.

Finally, with t_a and W optimised, the dependence of $NE\Delta\eta$ on plate length has been investigated. From these simulations it was observed that for any given minimum shear rate, an optimum plate length exists. This optimum length corresponds to the minimum value of ξ_0, where $\Delta\xi_{noise}$ is consequently at it lowest value. The optimum device configuration is therefore achieved by setting an arbitrarily fixed value of t_b and

then identifying the optimum plate length using iterative techniques, with t_a set at its maximum value and W at its minimum value at each point in this iteration.

The above methodology has been applied to calculate the optimum viscometer configuration for measurement of whole un-adulterated human blood, over a range of minimum shear rates. The results of these calculations, assuming a measurement bandwidth of $\Delta f = 50\text{Hz}$, are shown in table II. These optimum configurations have been applied to calculate the mechanical noise limited $\text{NE}\Delta\eta$. In each case, $\text{NE}\Delta\eta$ is calculated across a range of shear rates from $\langle\dot{\gamma}_0\rangle$ up to the assumed maximum rms

shear rate of $\langle\dot{\gamma}_{\max}\rangle = 1000\text{s}^{-1}$.

TABLE II Optimum viscometer configuration for a measurement bandwidth of $\Delta f = 50\text{Hz}$. The stated values of η_0 are calculated at associated damping ratio ξ_0 with both η_0 and ξ_0 being calculated at the stated $\langle\dot{\gamma}_0\rangle$.

$\langle\dot{\gamma}_0\rangle$	L	W	t_a	t_b	H	η_0	ξ_0	m_{eff}	k_s	V_0	V_1
(s^{-1})	(μm)	(μm)	(μm)	(μm)	(μm)	$(\text{Pa}\cdot\text{s})$	$(\times 10^{-3})$	$(\times 10^{-12}\text{kg})$	$(\text{N}\cdot\text{m}^{-1})$	(V)	(V)
0.1	180	41	0.01	0.05	629	0.033	0.49	2.6	0.7	100	49.0
0.2	410	37	0.01	0.05	533	0.024	0.42	5.3	1.9	100	49.2
0.5	1000	32	0.01	0.05	407	0.016	0.36	11.2	6.9	100	49.4
1.0	1000	27	0.01	0.05	274	0.012	0.40	9.2	12.5	100	49.4

The predicted performance as a function of shear rate, assuming a measurement bandwidth of 50Hz, is shown in figure 2.

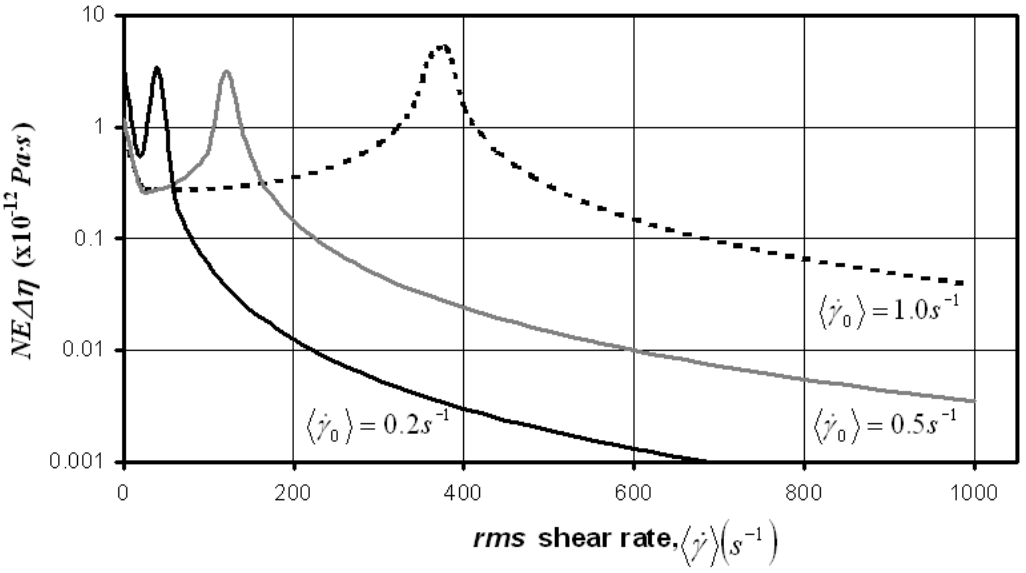

Figure (2) Mechanical noise limited $\text{NE}\Delta\eta$ as a function of the rms shear rate for the measurement of the viscosity of whole unadulterated human blood. Traces are shown for increasing $\langle\dot{\gamma}_0\rangle$ for a $\text{Au}-\text{SiN}$ plate structure using the optimum configuration shown in table II at a measurement bandwidth of 50Hz.

The distinct resonance peak on each curve suggests that, the dependence of $\text{NE}\Delta\eta$ on the applied shear rate is heavily influenced by the thermal-mechanical noise profile. Due to the small time shift associated with the predicted mechanical noise

limited $\mathrm{NE}\Delta\phi$ (noise equivalent change in phase angle,) the performance of the viscometer is expected to be limited by electronic noise within the detection circuitry. For example, at a measurement bandwidth of $50\mathrm{Hz}$, over a shear range of $0.2\mathrm{s}^{-1} \geq \langle \dot{\gamma}_0 \rangle \geq 1000\mathrm{s}^{-1}$, a mechanical noise limited value of $\mathrm{NE}\Delta\eta = 14.1\times10^{-12}\,\mathrm{Pa}\cdot\mathrm{s}$ is predicted. This corresponds to a change in phase angle of $\mathrm{NE}\Delta\phi = 6.3\times10^{-12}\,\mathrm{rad}$, which requires a time measurement resolution of $5.0\times10^{-18}\mathrm{s}$.

The electronic noise limited performance has been evaluated by imposing a minimum time measurement resolution of $50\,\mathrm{fs}$.[36] Since both $\mathrm{NE}\Delta\eta$ and η_{eff} vary with the applied shear rate, the predicted electronic noise limited performance is presented in terms of a fractional noise equivalent viscosity change, $\mathrm{NE}\Delta\eta/\eta_{\mathrm{eff}}$. The predicted $\mathrm{NE}\Delta\eta/\eta_{\mathrm{eff}}$ is at its highest value at the resonance peak and the stated value has been evaluated at this point. The results of these calculations, over a range of shear rates, are shown in table III.

TABLE III Electronic noise limited performance at a measurement bandwidth of $\Delta f = 50\text{Hz}$. Results calculated for using the optimum viscometer configuration shown in table II. The stated value of $\text{NE}\Delta\eta/\eta_{\text{eff}}$ corresponds to the highest value within the relevant shear range $\langle\dot{\gamma}_0\rangle \rightarrow \langle\dot{\gamma}_{\max}\rangle$.

$\langle\dot{\gamma}_0\rangle$	$\text{NE}\Delta\eta/\eta_{\text{eff}}$				
(s^{-1})	(%)				
	$\langle\dot{\gamma}_{\max}\rangle = 50\text{s}^{-1}$	$\langle\dot{\gamma}_{\max}\rangle = 100\text{s}^{-1}$	$\langle\dot{\gamma}_{\max}\rangle = 250\text{s}^{-1}$	$\langle\dot{\gamma}_{\max}\rangle = 500\text{s}^{-1}$	$\langle\dot{\gamma}_{\max}\rangle = 1000\text{s}^{-1}$
0.1	0.20	0.60	4.28	16.03	64.58
0.2	0.02	0.10	0.76	2.87	11.61
0.5	0.01	0.01	0.06	0.25	1.07
1.0	0.02	0.02	0.02	0.02	0.11

Simulations have also been conducted to investigate the relationship between the phase angle and the fluid viscosity. The phase angle is not simply related to the fluid viscosity but is also dependent on ω_E. The relationship between the phase angle and the fluid viscosity was therefore initially considered at several fixed values of ω_E.

As an example, the micro-mechanical viscometer optimised for a minimum shear rate of 0.1s^{-1} is considered. The results of these simulations, shown in figure 3, suggest that, for each fixed value of ω_E, a linear relationship will exist between ϕ and η_{eff}. From this it is inferred that, for any specific shear rate, a good linearity of response may be expected across the full measurement range of the device.

Figure (3) ϕ as a function of η_{eff} at a measurement bandwidth of $\Delta\text{f} = 50\text{Hz}$, assuming a minimum shear rate of $\langle \dot{\gamma}_0 \rangle = 0.1\text{s}^{-1}$.

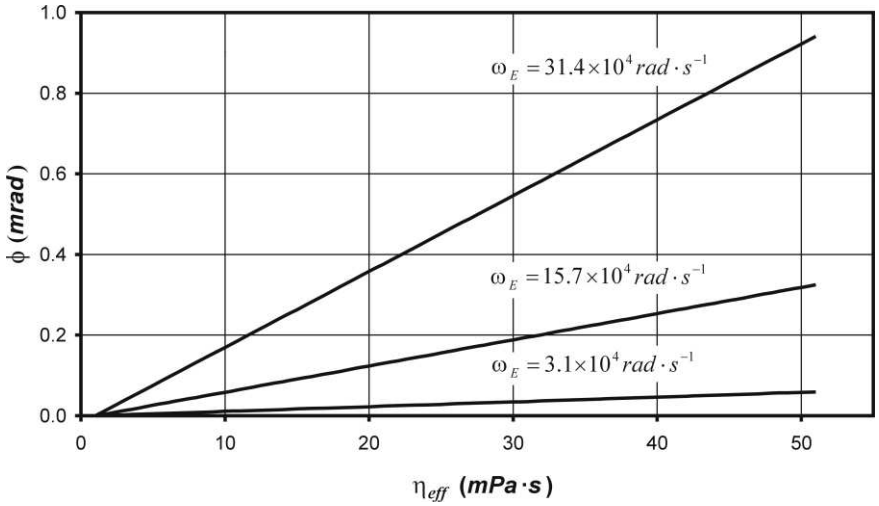

In order to derive a measurement of the phase angle that is independent of the driving frequency we consider the normalised phase angle ϕ/ω_E. Further analysis of our results suggest that a linear relationship exists between ϕ/ω_E and η_{eff}. In addition, it was found that for any given value of η_{eff}, the resulting value of ϕ/ω_E is constant irrespective of the applied driving frequency.

5 Discussion

The measurement resolution of the viscometer, quantified in terms of $\mathrm{NE}\Delta\eta/\eta_{eff}$, decreases as $\dot{\gamma}_{min}$ is increased. This is attributed to the reduction in $\Delta\xi_{noise}$, that results from a reduction in ξ_0 as H is allowed to increase. In addition, for any given $\langle\dot{\gamma}_0\rangle$, $\mathrm{NE}\Delta\eta/\eta_{eff}$ increases as the range of shear rate is increased. Therefore as the range of shear rates over which measurements are taken increases, the measurement resolution of the device is expected to decrease. A trade-off therefore exists between the required measurement resolution and the available range of shear.

In all optimisation and performance calculations, the effect of a change in ambient conditions has been neglected. The two main areas of concern have been identified as a change in the ambient temperature and a change in the ambient air pressure. A change in ambient temperature has the potential to cause bending of the bi-material plate due to the different thermal expansion coefficients of the two layers. However, due to the inherent rigidity of the plate structure, it seems reasonable to assume that no significant bending will occur due to a change in ambient temperature.

The effect of a change in ambient pressure is however somewhat more uncertain.

An initial assumption was made that the fluid viscosity will be independent of the ambient air pressure. By applying this initial assumption to equation (11) and (12), it was assumed that, to a first approximation, both ξ_0 and $\Delta\xi_{signal}$ are independent of P_{air}. These assumptions are however only valid assuming small σ.

In order to assess the significance of variations in P_{air} on the performance of the proposed viscometer, we now look at the magnitude of the change in signal, $\Delta\phi$, with changes in P_{air}. Applying the optimum viscometer configuration shown in table II for $\dot{\gamma}_{min} = 1.0 s^{-1}$, and introducing a change in ambient air pressure of $\Delta P_{air} \approx \pm 0.1 kPa$, a change phase angle of $\Delta\phi = \pm 4 \times 10^{-17} rad$ is predicted. Therefore, when measuring the viscosity of whole unadulterated human blood, the variation in ϕ with P_{air} may justifiably be considered to be negligible.

6 Conclusion

Close attention was paid to the optimisation of the viscometer configuration and a methodology for determining the optimum configuration for the micro-mechanical viscometer has been identified. It is predicted that, the viscometer performance will be limited by electronic noise within the detection circuitry and not by thermal mechanical displacement noise.

From the predicted electronic noise limited performance values it can be concluded that, the proposed micro-mechanical viscometer promises to provide a

measurement resolution that will at least match, if not exceed that of, conventional measurement technology. For example, for viscosity measurements taken over a shear range of 1s^{-1} to 1000s^{-1} a value of $\text{NE}\Delta\eta/\eta_{\text{eff}} \approx 0.1\%$ is predicted for a sampling bandwidth of 50Hz (i.e. 20ms per measurement). A linear measurement response is also predicted.

In addition, the proposed micro-mechanical viscometer requires smaller sample volumes and offers a faster measurement time than even the most advanced capillary-tube based measurement techniques. The proposed micro-mechanical viscometer has the additional advantage of providing a compact, self-contained design, which is ideally suited to the development of a low cost, disposable, sampling and measurement system for whole unadulterated human blood.

References

1 G. de Simone, R.B. Devereux, S. Chen, M.H. Alderman, S.A. Atlas and J.H. Laragh, Relation of blood viscosity to demographic and physiologic variables and to cardiovascular risk factors in apparently normal adults, Circulation, 81 (1990), 107-117.

2 R.S. Rosenson, Viscosity and ischemic heart disease, J. Vasc. Med. Biol, 4 (1993), 206-212.

3 G. Marinakis and S.Tsangaris, A new capillary vision system for whole blood and plasma viscosimetery in dislipidemia and hypertension, 11th Conference of the ESB, Toulouse, France July 8-11 1998, 169.

4 S. Kim, Y.I. Cho, A.H. Jeon, B. Hogenauer, and K.R. Kensey, A new method for blood viscosity measurement, J. Non-Newtonian Fluid. Mech., 94 (2000), 47-56.

5 S. Wang, A.H. Boss, K.R. Kensey and R.S. Rosenson, Variations of whole blood viscosity using Rheolog™ – a new scanning capillary viscometer, Clinica Chimica Acta, 332 (2003), 79-82.

6 S. Kim, Y.I. Cho, K.R. Kensey, R.O. Pellizzari and P.R.H. Stark, A scanning dual-capillary-tube viscometer, Rev. Sci. Instrum, 71 (2000), 3188-3192.

7 S. Shin, S. Lee and D-Y Keum, A new mass-detecting capillary viscometer, Rev. Sci. Instrum., 72 (2000), 3127-3128.

8 S. Shin and D-Y. Keum, Measurement of blood viscosity using mass-detecting sensor, Biosensors and Bioelectronics, 17 (2002), 383-388.

9 K. Hausler, W.H. Reinhart, P. Schaller, J. Dual, J. Goodbread and M. Sayir, A newly designed oscillating viscometer for blood viscosity measurements, Biorheology, 33 (1996), 397-404.

10 A.I. Romoscanu, M.B. Sayir, K. Hausler and C. Servais, High frequency probe for the measurement of the complex viscosity of liquids, Meas. Sci. Technol, 14 (2003), 451-462.

11 M.J. Vellekoop, Acoustic wave sensors and their technology, Ultrasonics, 36 (1998), 7-14.

12 H.L. Bandey, R.W. Cernosek, W.E. Lee III and L.E. Ondrovic, Blood rheological characterization using the thickness-shear mode resonator, Biosensors and Bioelectronics, 19 (2004), 1657-1665.

13 E.v.d. Burg, Z. Kojro and W. Grill, Synchronous determination of the rheological and acoustic properties of fluids using an oscillating fiber sensor and an ultrasonic microscope with phase contrast, Ultrasonics, 36 (1998), 483-490.

14 M.K. Andrews and P.D. Harris, Damping and gas viscosity measurements using a microstructure, Sensors and Actuators, A49 (1995), 103-108.

15 P.I. Oden, G.Y. Chen, R.A. Steele, R.J. Warmack and T. Thundat, Viscous drag measurements utilizing microfabricated cantilevers, Appl. Phys. Lett, 68 (1996), 3814-3816.

16 S. Boskovic, J.W.M. Chon, P. Mulvaney and J.E. Sader, Rheological measurements using microcantilevers, J. Rheol., 46 (2002), 891-899.

17 A. Vidic, D. Then, Ch. Ziegler, A new cantilever system for gas and liquid sensing, Ultramicroscopy, 97 (2003), 407-416.

18 A. Agoston, F. Keplinger and B. Jakoby, Evaluation of a vibrating micro-machined cantilever sensor for measuring the viscosity of complex organic liquids, Sensors and Actuators, Axxx (2005), xxx-xxx. (IN PRESS)

19 R.E. Jones and D.P. Hat, On interactions between substrates and SPM cantilevers immersed in fluids, Tribology International, 38 (2005), 355-361.

20 D.G. Fertis, Mechanical and structural vibrations, J. Wiley & Sons, New York, 1995.

21 F.L. Singer and A. Pytel, Strength of materials: 3rd Ed, Harper and Row, New York, 1980

22 R.J. Roark and W.C.Young, *Roark's formulas for stres*s and strain 6th Ed., McGraw Hill, New York, 1989.

23 J.P. Den Hartog, Advanced strength of materials, McGraw Hill, New York, 1952.

24 R.F. Steidel, An introduction to mechanical vibrations: 3rd Ed., Wiley, New York, 1989.

25 J.J. Blech, On isothermal squeeze films, J. Lubr. Technol., 105 (1983), 615-620.

26 M.E. O'Neil and F Chorlton, Viscous and compressible fluid dynamics, Ellis Horwood Ltd, Chichester, 1989.

27 T.B. Gabrielson. Mechanical–Thermal noise in micromachined acoustic and vibration sensors. IEEE Trans. Electron. Dev. 1993; 40:903-9.

28 M. Kajima, N. Kusumi, S. Moriwaki and N. Mio. Wide-band measurement of mechanical thermal noise using a laser interferometer. Phys. Lett. A. 1999; 264:251-6.

29 P.R. Saulson. Thermal noise in mechanical experiments. Phys. Rev. D 1990; 42:2437-45.

30 R. Puers and D. Lapadatu, Electrostatic forces and their effects on capacitive mechanical sensors, Sensors and Actuators, A56 (1996), 203-210.

31 P.B. Chu, P.R. Nelson, M.L. Tachiki and K.S.J. Pister. Dynamics of polysilicon parallel-plate electrostatic actuators. Sensors and Actuators 1996; A52:216-20.

32 K.E. Petersen. Dynamic micromechanics on Silicon: Techniques and devices. IEEE Trans. Electron. Dev 1978; 25:1241-50.

33 M.M. Cross, Rheology of Non-Newtonian fluids: A new flow equation for pseudoplastic systems, J. Colloid Interface Sci., 20 (1965), 417–437.

34 G.Winther, K. Almdal and O. Kramer, Determination of polymer melt viscosity by squeezing flow with constant plate viscosity, J. Non-Newtonian Fluid Mech., 39 (1991), 119-136.

35 C.W. Macosko, Rheology: principles, measurements, and applications, Wiley-VCH Inc., New York, 1994.

36 Quartzlock UK Ltd, Frequency, phase and phase noise measurement system A7-A & A7-M, Detailed technical specification-Issue 1A.